Synthesis, Structural Characterization, Solvatochromism, and Electrochemistry of Tetra-Osmium Carbonyl Clusters Containing Azo-Ligands

Yat Li,[a] Zhen-Yang Lin,[b] and Wing-Tak Wong*[a]

Keywords: Electrochemistry / Solvatochromism / Azo-compounds / Osmium / Cluster compounds

The reaction of $[Os_4(\mu\text{-}H)_4(CO)_{12}]$ with 4-(2-pyridylazo)-*N*,*N*-dimethylaniline (PNNDA) in dichloromethane afforded the new clusters $[Os_4(\mu\text{-}H)_4(CO)_{11}\{NC_5H_4(N{=}N)C_6H_4NMe_2\}]$ (**1**) and $[Os_4(\mu\text{-}H)_4(CO)_{10}\{\eta^2\text{-}NC_5H_4(N{=}N)C_6H_4NMe_2\}]$ (**2**) in 34% and 15% yields, respectively. Upon heating in toluene under reflux, compound **1** converted into **2** in 80% yield. The MLCT transition of compound **2** shows strong solvent dependency, displaying unusually large positive solvatochromism in different organic solvents. Treatment of $[Os_4(\mu\text{-}H)_4(CO)_{12}]$ with 2-(5-bromo-2-pyridylazo)-5-(diethylamino)-phenol (Br-PADAP) in dichloromethane gives $[Os_4(\mu\text{-}H)_3(CO)_{10}\{\mu\text{-}\eta^3\text{-}Et_2NC_6H_3(O)(N{=}N)C_5NH_3Br\}]$ (**3**). The O–H bond activation is observed and the azo-ligand behaves as a five-electron donor. The clusters $[Os_4(\mu\text{-}H)_2(CO)_{10}\{\mu\text{-}\eta^3\text{-}NC_5H_4(N{=}N)C_5H_4N\}]$ (**4**) and $[Os_4(\mu\text{-}H)_4(CO)_{10}\{\mu\text{-}\eta^2\text{-}NC_5H_4(N{=}N)C_5H_4N\}]_2$ (**5**) were isolated from the reaction of $[Os_4(\mu\text{-}H)_4(CO)_{10}(NCMe)_2]$ with 2,2′-azopyridine and 3,3′-azopyridine, respectively. In compound **4**, both pyridine and azo nitrogen atoms were found to coordinate to the cluster core. Dehydrogenation was also observed in this compound. For compound **5**, two tetra-osmium metal cores were connected by two azo ligands through their pyridyl nitrogen atoms to form a novel cyclic structure. The redox properties of the compounds described herein were investigated by means of cyclic voltammetry and controlled potential coulometry. Both compound **2** and **5** exhibit a reversible cathodic wave, which indicates that they undergo addition of one electron without significant structural changes. Furthermore, compound **5** displays an electronic interaction between two redox centers, the extra electrons are believed to delocalize throughout the cyclic structure.

Introduction

The activation of strong multiple-bonded organic substrates using polynuclear metal complexes is an interesting facet of cluster reactivity. The cleavage of N=N bond in organic diazenes to give metal imido (nitrene) complexes is an important chemical transformation.[1−5] Metal imido complexes have been shown to be potential intermediates for metal-prompted organic transformations involving the formation of nitrogen-carbon bonds. As a result, the chemistry of carbonyl clusters containing azo ligands has been extensively studied in recent years.[6−18] Previously, we reported that $[Os_3(CO)_{10}(NCMe)_2]$ reacts with 2-(5-bromo-2-pyridylazo)-5-(diethylamino)phenol at room temperature to give $[Os_3(CO)_{10}\{\mu\text{-}N(H)(C_5H_3NBr)\}\{\mu\text{-}N(C_{10}H_{13}NO)\}]$,[19] containing two types of amido moieties, in which N=N cleavage of the azo ligand was observed. In an attempt to synthesize tetra-osmium imido complexes by the N=N cleavage of azo ligands, we were able to prepare some new tetra-osmium carbonyl clusters containing azo ligands. However, no cleavage of the N=N bond of these compounds by thermal or photochemical methods was observed. These compounds exhibit interesting solvatochromism and electrochemistry. The redox behavior of the clusters $M_3(CO)_{12}$ (M = Fe, Ru, Os) has been extensively studied.[20−23] To the best of our knowledge, the electrochemical behavior of tetra-osmium carbonyl clusters is rarely reported. The correlation between the structure and the redox properties of these compounds was also described.

[a] Department of Chemistry, The University of Hong Kong, Pokfulam Road, Hong Kong, P. R. China
Fax: (internat.) + 852-2547/2933 or + 852-2857/1586
E-mail: wtwong@hkucc.hku.hk
[b] Department of Chemistry, The University of Science and Technology, Clear Water Bay, Hong Kong, P. R. China

Results and Discussion

The preparation of compounds **1**−**5** is summarized in Scheme 1 and Scheme 2. These compounds have been fully characterized by elemental analyses, infrared, ^{1}H NMR, and mass spectroscopic methods. The infrared spectra of compounds **1**−**5** revealed that only terminal carbonyl ligands were present, and the mass spectra exhibit molecular ion envelopes that agree with the formulae of the compounds, with stepwise loss of terminal carbonyl ligands. Their molecular structures were established by single crystal X-ray diffraction analyses.

The molecular ion peak was not observed in the mass spectrum of **1** due to fragmentation during the ionization process. However, it exhibits an intense daughter peak at m/z = 1073 attributed to $[M^+ - PNNDA]$, and is followed by peaks corresponding to the successive loss of carbonyl groups. The chelation of the azo ligand is supported by the ^{1}H NMR spectroscopic data. The ^{1}H NMR spectrum of **1** shows two sets of multiplets for the aromatic protons at δ = 6.84−8.01. Two sets of singlets at δ = 2.04 and 1.67 correspond to the methylene protons of the azo-ligand. The

  1434−1948/01/1212−3163 $ 17.50+.50/0

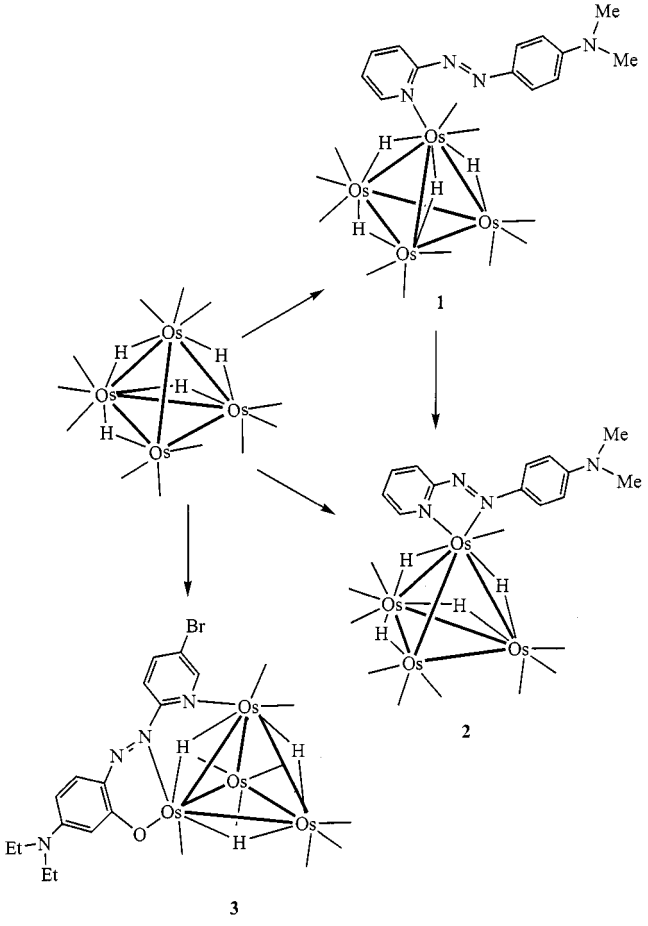

Scheme 1

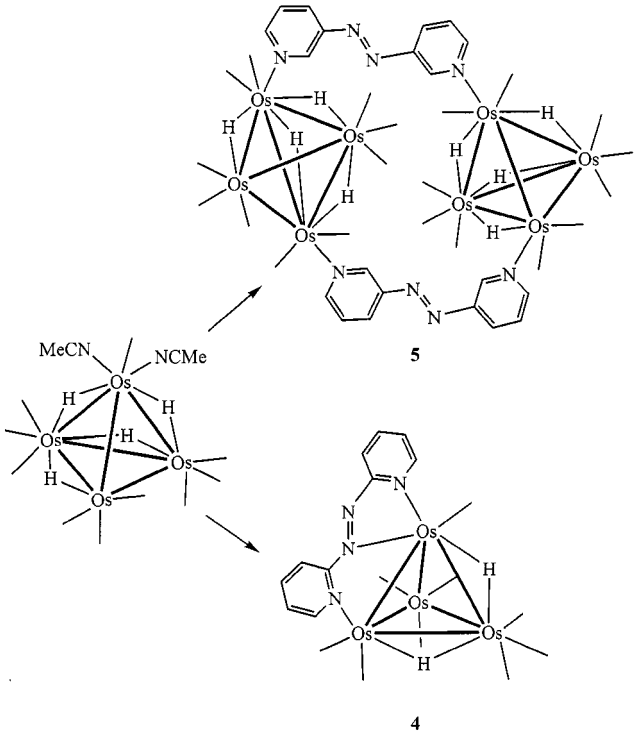

Scheme 2

^{1}H NMR cannot give a clear assignment of four hydrides in the tetra-osmium core due to the fluxional behavior of hydrides at room temperature, which is common in tetra-osmium systems.[24−25] Therefore, a variable-temperature ^{1}H NMR study from 233 to 298 K was conducted for **1**. At 233 K, the broad hydride peaks resolved into two sets of sharp singlet peaks at $\delta = -18.10, -18.63, -24.01$ and at $\delta = -16.93, -17.95, -18.86, -25.53$, with an integral ratio of 2:1:1 and 1:1:1:1, respectively. This indicates the presence of two possible isomers in solution, namely **1a** and **1b**, due to a different bridging hydride disposition. As the temperature is raised to 253 K, the ratio of **1b** to **1a** gradually increases from 0.4 to 0.5. This suggests that isomer **1a** is more favored in solution at a higher temperature.

The molecular structure of **1** is depicted in Figure 1 and selected bond lengths, and angles are summarized in Table 1. Four osmium atoms define a distorted tetrahedron with eleven carbonyl ligands terminally bonded to the metal centers. The Os(2)−Os(3) and Os(2)−Os(4) [2.819(1) and 2.809(1) Å] lengths of compound **1** are comparable to the corresponding values observed in the parent cluster $[Os_4(\mu\text{-}H)_4(CO)_{10}(NCMe)_2]$.[26] The hydride bridged Os−Os bonds are significantly elongated,[27] within the range [2.928(1)-3.022(1) Å]. The hydrides bridging the Os(1)−Os(3) and Os(1)−Os(4) are chemically equivalent, which give a sharp singlet with double integral value in low temperature ^{1}H NMR spectra. Hence, it is believed that the solid-state structure of **1** obtained by X-ray crystallography is the structure of isomer **1a**. The azo-ligand terminally coordinated to Os(1) through the pyridyl nitrogen N(1) with a mirror plane bisects along the azo ligand and Os(1) atom. The Os(1)−N(1) bond length [2.17(2) Å] is not significantly different from the equivalent Os−N distance found in other osmium-pyridine containing complexes.[28] The N(2)−N(3) bond [1.26(2) Å] is slightly lengthened compared to other azo ligands in the tri-osmium system[29] due to the electron donating aniline group, consistent with its assignment as a N−N double bond. The torsion angle defined by C(16)−N(2)−N(3)−C(17) is 178(2)°, indicating that the *trans* configuration of the ligand remains almost intact upon coordinating to the cluster framework. The dihedral angle between the pyridyl and phenyl rings is 8.08°.

Upon heating under reflux in toluene, compound **1** converted into **2** in 80% yield. Substitution of a carbonyl ligand on Os(1) by azo nitrogen was observed. The ^{1}H NMR of **2** is similar to **1**, with three broad peaks in hydride region. A variable-temperature ^{1}H NMR study was conducted for **2** from 223 to 298 K. At 223 K, the broad peaks resolved into four sets of sharp hydride signals, each with the relative intensity 1:1:1:1, indicating the presence of four isomers (namely **2a**, **2b**, **2c**, and **2d**) in solution, see Figure 2. The ratio of **2a/2b/2c/2d** is 1:2:5:8. The molecular structure of compound **2** is illustrated in Figure 3 and the relevant bond parameters are listed in Table 1. A chloroform molecule, as a solvent of crystallization, is present in the crystal lattice. The basic metal architecture of **1** is retained in compound **2**. The azo ligand coordinated to Os(1) through the pyridyl nitrogen N(1) and the azo nitrogen N(3) atom.

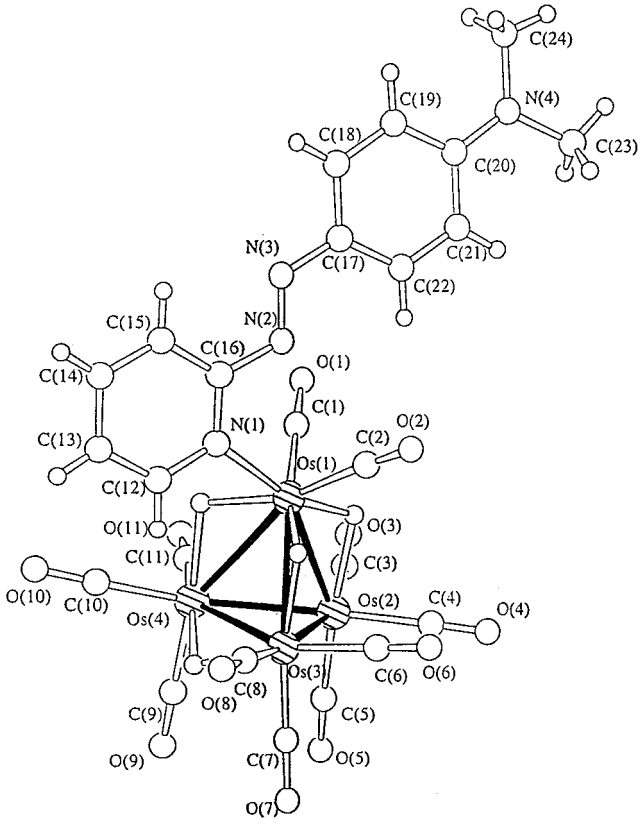

Figure 1. The molecular structure of clusters $[Os_4(\mu\text{-}H)_4(CO)_{11}\{NC_5H_4(N{=}N)C_6H_4NMe_2\}]$ (**1**) showing the atom numbering scheme

Os(1)−N(1)−C(15)−N(2)−N(3) form a metallacyclic five-membered ring with a mean deviation of 0.022Å from the least-square plane. The N(1)−Os(1)−N(3) coordination is asymmetric, with Os(1)−N(1) and Os(1)−N(3) bond lengths of 2.078(6) Å and 2.111(7), respectively, and a N(1)−Os(1)−N(3) angle of 75.0(3)°. The N(2)−N(3) length [1.290(9) Å] is almost identical to **1**, indicating a retained double bond character. Upon coordination of azo nitrogen, the pyridyl and phenyl rings are twisted with respect to each other to a greater extent, with a dihedral angle of 11.8°.

The molecular structure of **3** is shown in Figure 4 and some important bond lengths and angles are listed in Table 1. The azo-ligand was found to bridge the edge Os(1)−Os(2) of the Os_4 distorted tetrahedron, affording a five-membered ring containing Os(1), Os(2), N(2), C(15), and N(1) and a six-membered ring containing Os(2), O(11), C(21), C(16), N(3), and N(2), respectively. These rings had a maximum deviation of 0.205 Å and 0.192 Å from the least-square planes, respectively. The dihedral angle between two metallacyclic rings is 25.5°. The Os(1)−Os(2) bond [2.7816(6) Å] is slightly shorter than the hydride bridged Os−Os bonds. The O−H bond cleavage is observed in **3**. This bonding mode of the azo ligand is very similar to that found in the tri-osmium cluster $[(\mu\text{-}H)Os_3(CO)_9\{\mu\text{-}\eta^3\text{-}Et_2NC_6H_3(O)(N{=}N)C_5NH_3Br\}]$.[29] The N(2)−N(3) bond length [1.32(1) Å] is comparable to the N=N bonds in **1** and **2**, indicating no involvement of the π-electrons of the N=N bond. The pyridyl and phenyl rings are highly twisted with respect to each other, with a dihedral angle of 60.3° due to the bond strain. The characteristic 60 cluster-valence electron count was observed with the azo-ligand acting as a five-electron donor. Only three bridging hydrides were found in the metal core, confirmed by ^{1}H NMR spectroscopy, with three sharp peaks of equal intensity observed in the hydride region.

The molecular structure of **4** is depicted in Figure 5 and the relevant bond lengths and angles are listed in Table 1. It has a structure similar to compound **2** in terms of ligand coordination, however, the involvement of the other pyridyl ring was observed. The coordination of the azo-ligand, acting as a six-electron donor, resulted in a pair of hydrides being eliminated rather than a carbonyl ligand being substituted. Such elimination is not commonly observed in osmium chemistry. The presence of only two hydrides on the metal core is supported by ^{1}H NMR spectroscopic data, with two sharp singlets of equal intensity observed in hydride region. The ligand bridged Os(1)−Os(3) bond length [2.8145(8) Å] is slightly shorter than the hydride bridged Os−Os bonds. Os(1)−Os(3)−N(4)−C(16)−N(3) and Os(1)−N(1)−C(15)−N(2)−N(3) form two metallacyclic five-membered rings, with a mean deviation of 0.034Å and 0.159Å, respectively, from the least square planes. The Os(3)−N(4) bond [2.18(1) Å] is significantly lengthened compared to Os(1)−N(1) bond [2.06(1) Å] and Os(1)−N(3) bond [2.05(1) Å], owing to the bond strain. The two pyridyl rings are not coplanar, with a dihedral angle upon coordination to the metal framework of 16.2° between them. The bite angle N(1)−Os(1)−N(3) of chelating azo-ligand is 75.3(5)°, which is comparable to **2** [N(1)−Os(1)−N(3) 75.0(3)°] and $[Os_3(CO)_{10}(bipy)]$ [N−Os−N 75.6(9)°].[30]

Although the ligand system of **5** is very similar to **4**, they have totally different reaction pathways towards the tetra-osmium cluster. The molecular structure of **5** is illustrated in Figure 6 and the relevant parameters are listed in Table 1. Four tetrahydrofuran molecules, as a solvent of crystallization, were found in the crystal lattice. Two tetra-osmium metal cores are connected by two azo-ligands through their pyridyl nitrogen atoms N(1) and N(4) to form a novel cyclic structure. A similar cyclic structure was observed in the tri-osmium cluster system.[31] Cluster **5** possesses a C_i symmetry, with the center of inversion at the central point of the square involving Os(3), Os(4), Os(3)*, and Os(4)*. The Os(1)−N(1) [2.18(2) Å] and Os(2)−N(4)* [2.13(2) Å] bond lengths are lengthened relative to other Os−N dative bonds because of the large steric hindrance in the cyclic structure. The two pyridyl rings are twisted with a dihedral angle of 24.5°. The two tetra-osmium sets of atoms with their associated carbonyl ligands do not approach each other very closely; the nearest contact is O(3)···O(3)* [5.48(3) Å] and the shortest Os···Os distance between clusters is Os(2)···Os(2)* [7.940(2) Å]. This novel cyclic structure opens the possibility of encapsulating some alkali or oxophilic metal ions. The supramolecular system so formed will be useful for the studies of redox active host towards metal ion sensing applications. The steric effect may be the main

Table 1. Selected bond lengths [Å] and angles [°] for compounds **1**−**5**

	1	**2**	**3**	**4**	**5**
Os(1)−Os(2)	2.928(1)	3.0080(4)	2.7816(6)	2.8718(8)	2.977(2)
Os(1)−Os(3)	2.985(1)	2.9781(4)	3.0117(6)	2.8145(8)	2.993(2)
Os(1)−Os(4)	3.022(1)	2.9753(4)	2.7903(6)	2.8742(8)	2.747(2)
Os(2)−Os(3)	2.819(1)	2.8202(4)	2.9896(6)	2.9089(8)	3.005(1)
Os(2)−Os(4)	2.809(1)	2.9425(5)	2.9224(7)	2.7494(8)	3.013(1)
Os(3)−Os(4)	2.954(1)	2.7857(4)	2.7655(6)	2.8477(8)	2.832(1)
Os(1)−N(1)	2.17(2)	2.078(6)	2.143(9)	2.06(1)	2.18(2)
Os(1)−N(2)	–	–	2.132(1)	–	–
Os(1)−N(3)	4.45	2.111(7)	–	2.05(1)	–
Os(2)−N(4)	–	–	–	–	2.13(2)
Os(3)−N(4)	–	–	–	2.18(1)	–
Os(2)−O(11)	–	–	2.138(7)	–	–
N(2)−N(3)	1.26(2)	1.290(9)	1.32(1)	1.34(2)	1.28(3)
C(12)−Br(1)	–	–	1.89(1)	–	–
Os(2)−Os(1)−Os(3)	56.95(3)	56.212(9)	61.99(1)	61.53(2)	60.44(4)
Os(2)−Os(1)−Os(4)	56.32(3)	58.91(1)	63.27(2)	57.17(2)	63.38(4)
Os(3)−Os(1)−Os(4)	58.92(3)	55.80(1)	56.78(2)	60.07(2)	58.94(4)
Os(1)−Os(2)−Os(3)	62.56(3)	61.36(1)	62.79(1)	58.27(2)	60.05(3)
Os(1)−Os(2)−Os(4)	63.54(3)	59.99(1)	58.51(1)	61.46(2)	54.59(4)
Os(3)−Os(2)−Os(4)	63.33(3)	57.77(1)	55.77(1)	60.35(2)	56.15(3)
Os(1)−Os(3)−Os(2)	60.49(3)	62.43(1)	55.22(1)	60.21(2)	59.51(4)
Os(1)−Os(3)−Os(4)	61.16(3)	62.05(1)	57.57(1)	61.01(2)	56.19(4)
Os(2)−Os(3)−Os(4)	58.16(3)	63.32(1)	60.89(2)	57.05(2)	62.07(4)
Os(1)−Os(4)−Os(2)	60.15(3)	61.10(1)	58.22(2)	61.37(2)	62.03(4)
Os(1)−Os(4)−Os(3)	59.93(3)	62.15(1)	65.65(2)	58.93(2)	64.87(4)
Os(2)−Os(4)−Os(3)	58.51(3)	58.91(1)	63.35(2)	62.60(2)	61.78(4)
Os(2)−Os(1)−N(1)	–	–	84.3(3)	–	98.8(6)
Os(1)−Os(2)−N(4)	–	–	–	–	147.7(6)
Os(4)−Os(1)−N(1)	99.7(5)	–	–	–	–
N(1)−Os(1)−N(3)	–	75.0(3)	–	75.3(5)	–
N(2)−Os(2)−O(11)	–	–	82.1(3)	–	–

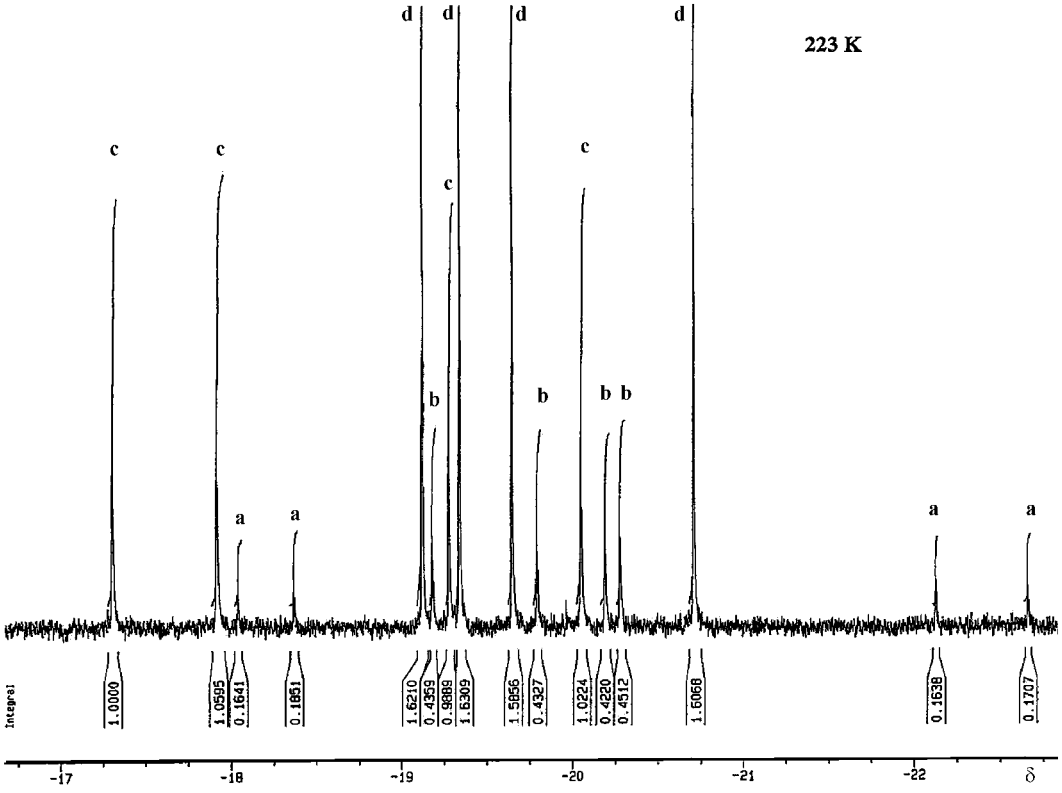

Figure 2. The low temperature (223 K) ^{1}NMR spectra of $[Os_4(\mu\text{-}H)_4(CO)_{10}\{\eta^2\text{-}NC_5H_4(N{=}N)C_6H_4NMe_2\}]$ (**2**) in the hydride region

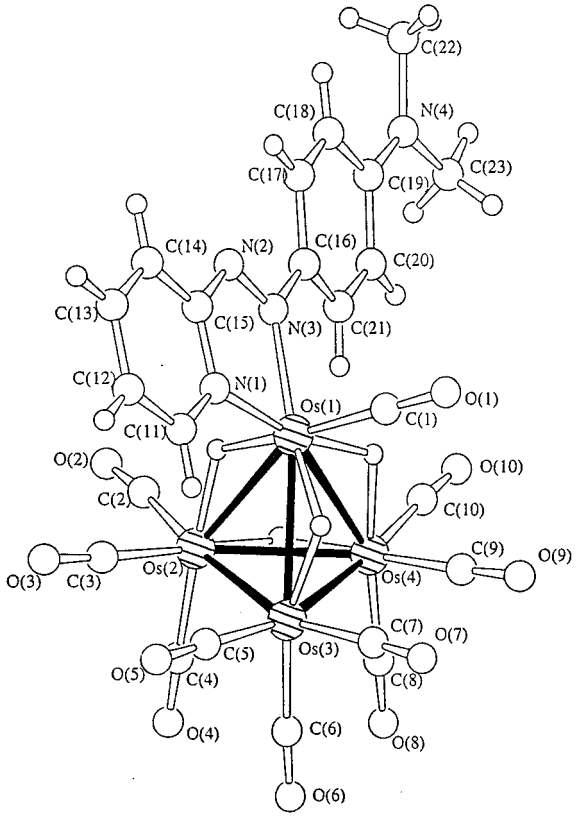

Figure 3. The molecular structure of clusters $[Os_4(\mu\text{-}H)_4(CO)_{10}\{\eta^2\text{-}NC_5H_4(N{=}N)C_6H_4NMe_2\}]$ (**2**) showing the atom numbering scheme

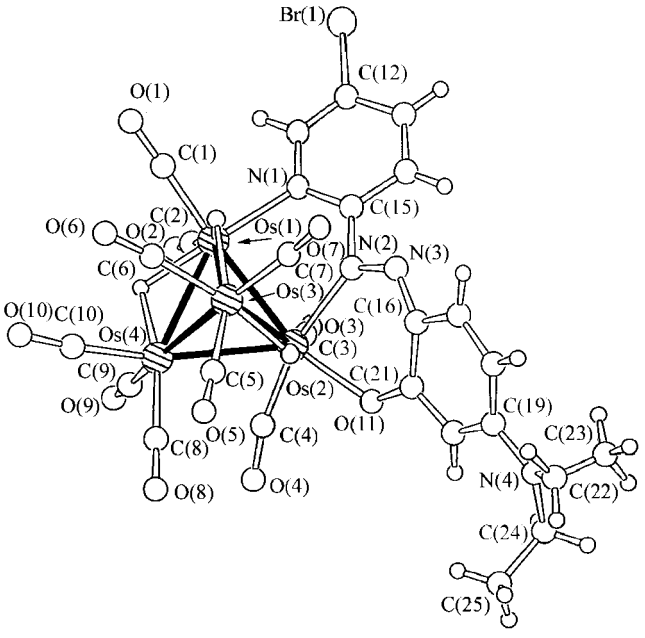

Figure 4. The molecular structure of clusters $[Os_4(\mu\text{-}H)_3(CO)_{10}\{\mu\text{-}\eta^3\text{-}Et_2NC_6H_3(O)(N{=}N)C_5NH_3Br\}]$ (**3**) showing the atom numbering scheme

reason for the cyclic structure not being observed in the reaction of 2,2′-azopyridine. 3,3′-Azopyridine provides a much larger separation between the two metal cores due to the direction of pyridine nitrogen lone pair electrons.

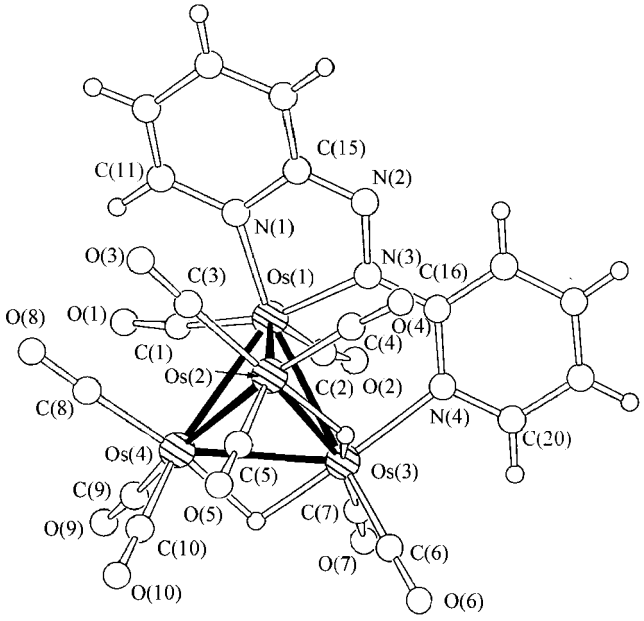

Figure 5. The molecular structure of clusters $[Os_4(\mu\text{-}H)_2(CO)_{10}\{\mu\text{-}\eta^3\text{-}NC_5H_4(N{=}N)C_5H_4N\}]$ (**4**) showing the atom numbering scheme

Solvatochromism

Compounds **1**−**5** show a variety of intense colors in the solid state, which prompted us to examine them by optical spectroscopy. Based on the experimental geometry, molecular orbital calculations at the B3LYP level of density functional theory were carried out for these compounds to examine the characteristics of the molecular orbitals in the frontier region. Similar to trinuclear osmium clusters,[32−33] the highest occupied molecular orbital (HOMO) of these compounds is mainly metal based, and the lowest unoccupied molecular orbital (LUMO) mostly based on the organic moiety.[34] The intense color of these compounds undoubtedly arises from a strong absorption due to metal-to-ligand charge transfer (M.L.C.T.) transitions.[32,34] These compounds exhibit solvatochromic absorptions in the visible region, contributed by changes in the metal-ligand bond polarity between the ground and excited states and specific solvent-solute and induced dipolar interaction.[35−40] The optical spectral parameters for a range of solvents are summarized in Table 2.

Compounds **1**−**3**, demonstrated a positive solvatochromism,[41−42] where the dipole moment of ground state (μ_g) is smaller than the excited state (μ_e). On MLCT transition, polar solvents were found to be better at stabilizing the excited state of the molecule. The red shift in absorption energies from *n*-hexane to dichloromethane was due to the increasing polarity of the organic solvents. The exceptionally large solvatochromism was observed in compound **2** (Figure 7), due to the smaller energy gap of HOMO−LUMO electronic transition. The contour plots of the lowest unoccupied (LUMO) and the highest occupied (HOMO) molecular orbitals of **2** are illustrated in Figure 8. The molecular orbital calculations showed that N(2) has a

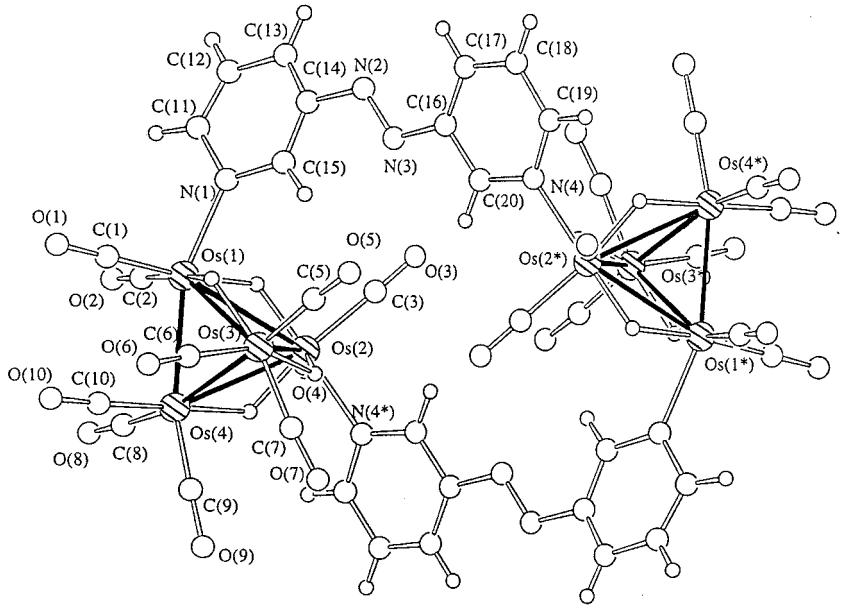

Figure 6. The molecular structure of clusters $[Os_4(\mu\text{-}H)_4(CO)_{10}\{\mu\text{-}\eta^2\text{-}NC_5H_4(N{=}N)C_5H_4N\}]_2$ (**5**) showing the atom numbering scheme

Table 2. Electronic absorption spectroscopic data for compounds **1**–**5**

Compounds	λ_{max} (nm) ε ($dm^3 \cdot mol^{-1} \cdot cm^{-1}$) *n*-hexane	acetone	dichloromethane
1	480[a]	497 (16000)	497 (18000)
2	504 (11000)	572 (15000)	577 (13000)
3	482 (5000)	522 (4000)	524 (4000)
4	613 (3000)	600 (2000)	607 (2000)
5	–	330 (34000)	306 (57000)

[a] Limited solubility for accurate determination of ε value.

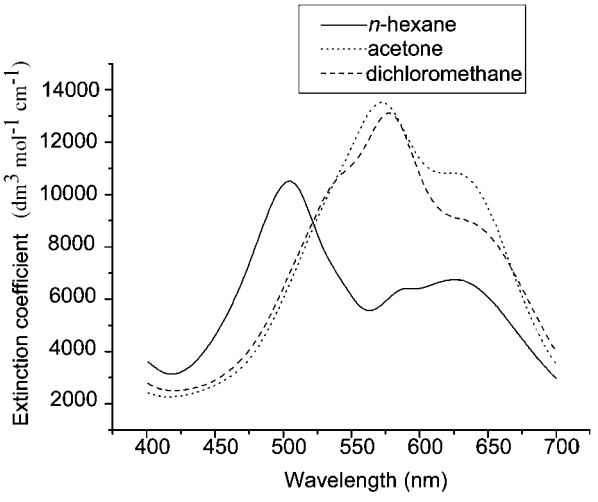

Figure 7. The electronic absorption spectrum of $[Os_4(\mu\text{-}H)_4(CO)_{10}\{\eta^2\text{-}NC_5H_4(N{=}N)C_6H_4NMe_2\}]$ (**2**) in a range of organic solvents

lone pair of electrons whose maximum electron density points away from the central cluster unit. This lone pair is greatly affected by the solvent environment. The interac-

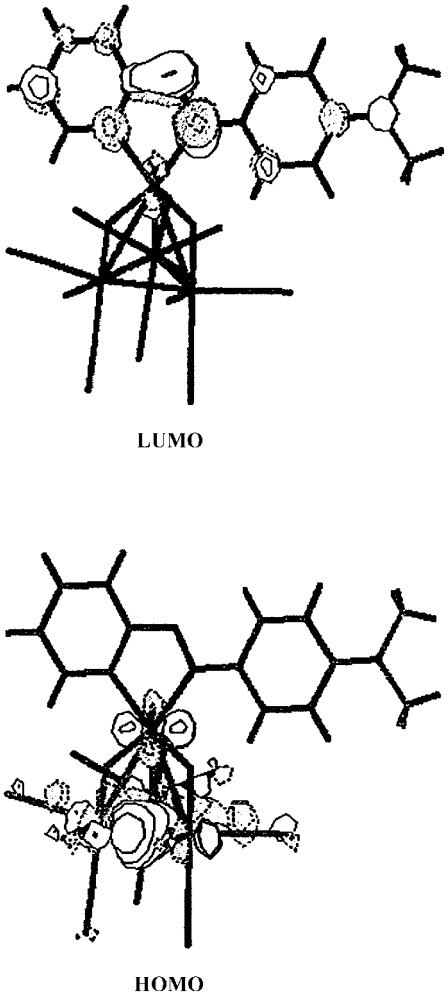

Figure 8. The contour plots of the lowest unoccupied- (LUMO) and the highest occupied (HOMO) molecular orbitals calculated for $[Os_4(\mu\text{-}H)_4(CO)_{10}\{\eta^2\text{-}NC_5H_4(N{=}N)C_6H_4NMe_2\}]$ (**2**)

tions with the polar solvents pull the electron density away from the N(2) center, lowering the orbital energy of the LUMO, which contains significant N(2)−N(3) π* character. As a result, the MLCT transition will shift to a lower energy (red shift) in polar solvents. Compound **2** has a much lower energy MLCT absorption than compound **1**. It is believed that more extensive ligand coordination to the cluster core leads to a smaller HOMO−LUMO energy gap.

Compound **4** showed some degree of solvent dependence; however, it was random with respect to the solvent polarity. Compound **4** had a low energy absorption band at around 600 nm due to the extensive coordination of ligand. Compound **5** exhibited a strong featureless intraligand π→π* absorption band at around 300 nm, along with an analogous band observed in the absorption spectrum of free ligand 3,3′-azopyridine under the same conditions. As shown in Table 1, some degree of negative solvatochromism shift was detected for **5**. Apart from π→π* transition, no indication of a low-energy band was attributed to an MLCT transition.

Electrochemistry

In order to investigate the redox properties of these new azo-ligands containing tetra-osmium compounds, the electrochemistry of compounds **1−5** was examined. Cyclic voltammetry and controlled potential coulometry were carried out at 298 K in a standard three-electrode system (glassy carbon/carbon cloth working electrode, platinum auxiliary electrode, and $Ag/AgNO_3$ reference electrode)[43] using a 0.1 M tetrabutylammonium hexafluorophosphate/dichloromethane solution as supporting electrolyte. The results of voltammetric experiments are summarized in Table 3.

Table 3. Electrochemical data for compounds **1−5**

Compounds[a]	Oxidation E_{pa2} [V][b]	E_{pa1} [V][b]	Reduction E_{pc1} [V][b]	E_{pc2} [V][b]
1	−	0.64	−1.25	−
2	0.93	0.49	(−0.94)[c]	−1.27
3	−	0.72	−1.17	−
4	−	0.52	−	−
5	−	0.55	(−1.06)[c]	−1.68

[a] ca. 10^{-3} M cluster in 0.1 M TBAHFP in dichloromethane at 298 K, the working electrode was a glassy carbon electrode, the auxiliary electrode and the reference electrode were a platinum wire and $Ag/AgNO_3$ (0V) under the same conditions, calibrated with ferrocene. Scan rate was 100 mVs^{-1}. − [b] E_{pa} and E_{pc} are the anodic and cathodic potentials, respectively. − [c] Values in parentheses are $E_{1/2}$, half-wave potential values.

Compound **1** exhibits an irreversible cathodic wave (E_{pc}) and anodic wave (E_{pa}) at −1.25 and 0.64 V vs. $Ag/AgNO_3$ in dichloromethane, respectively. Applying a working potential (E_w) at −1.4 V, controlled potential coulometry showed that two faraday/mole of **1** was involved in this reduction step. On the basis of the relative peak currents of the cathodic and anodic waves, the oxidation process is assigned as a one-electron step. Two-electron addition to compound **1** is believed to afford a 62e compound, which would be unstable, with consequent metal−metal bond cleavage, leading to metal carbonyl fragments of lower nuclearity. It conforms to a ECEC or EEC mechanism.[44]

Compounds **1** and **2** have the same ligand system, their cyclic voltammograms were expected to be similar. Interestingly, the incorporation of the azo group in the cluster framework led to great changes in the electrochemical behavior of **2**. The cyclic voltammograms of **2** consist of a reversible and an irreversible cathodic wave at −0.94 and −1.27 V, respectively. Controlled potential coulometry at the first reduction step (E_w = −1.09 V) indicates that this cathodic process consumes 1 faraday/mole of **2**. Analysis of the cyclic voltammetric responses relating to the cathodic peak of **2**, with scan rate varying from 50 to 500 mVs^{-1}, indicates that the peak current ratio i_{pa}/i_{pc} remains close to unity. The current function (proportional to $i_{pc}/v^{1/2}$) is essentially constant and the peak-to-peak separation lies between 80−100 mV. This trend is parallel with the ferrocene under the same experimental conditions. Thus, we assume that the first reduction step proceeds by an essentially reversible electron transfer process. This implies that any structural change of **2** accompanying the single-electron transfer is chemically reversible and rapid with respect to the time scale of the electrochemical experiment. The irreversible nature of the second cathodic wave showed that the reduction of compound **2** followed an EEC mechanism. In addition, two anodic waves at 0.49 and 0.93 V were found. The similarity of the relative peak heights for the waves within a given voltammogram points to the same number of electrons being involved in the oxidation and reduction of **2**. Two irreversible one-electron oxidations in **2** were assigned to follow the ECEC process. There is a 310 mV positive and 150 mV negative shift upon coordination of azo group in cathodic and anodic wave values, respectively. It shows that both reduction and oxidation processes are more likely to occur. It is believed that the extensive ligand coordination lowers the HOMO−LUMO energy gap and hence gives a lower redox potential for compound **2**. This is consistent with the UV/Vis spectroscopic data. Furthermore, it is reasonable to suggest that the reversible step of **2** is due to the presence of a metallacyclic five-membered ring unit.

The cyclic voltammograms of **3** contained an irreversible cathodic wave at E_{pc} = −1.17 V vs. $Ag/AgNO_3$, along with a small return oxidation at −0.56 V. The region where the weak oxidation wave appears was initially empty, with the wave appearing after the cathodic wave was traversed. The ΔE_p values remained virtually unchanged on varying the scan rates from 50 to 1000 $mV \cdot s^{-1}$. An irreversible anodic wave is also located at E_{pa} = 0.72 V. The irreversible nature of both oxidation and reduction presumably derives from an irreversible chemical reaction that follows the redox reaction (EC process). Controlled potential coulometry was run at 0.87 V for **3**, showing that one electron is removed for each molecule. Based on the relative peak heights, the cathodic wave is tentatively assigned to have consumed two electrons. For compound **4**, only one irreversible anodic wave was located at E_{pa} = 0.54 V vs. $Ag/AgNO_3$ within the

solvent limit. Controlled potential coulometry at the oxidation step (E_w = 0.67 V) shows that the anodic process consumes one electron per molecule. Compounds **3** and **4** have a similar ligand disposition, however, the former is much harder to oxidize than the latter due to the presence of a strong electron-withdrawing bromine ligand. Moreover, although compound **4** is extensively coordinated by the azo-ligand, the oxidation potential is comparable to **2**. This suggested that the aniline is an effective electron-donating ligand that makes oxidation easier.

Compound **5** is a cyclic structure consisting of two tetra-osmium metal cores connected by two azo-ligands. Although compounds **1** and **5** have a similar ligand system, they show different redox behavior. It is believed that there is an electronic interaction between two redox centers. The cyclic voltammogram of **5** is shown in Figure 9. A quasi-reversible and an irreversible cathodic wave were observed at E_{pc} = −1.06 and −1.68 V vs. $Ag/AgNO_3$. In addition, an irreversible anodic wave occurred at E_{pa} = 0.55 V. Applying a working potential at 0.8 V, controlled potential coulometry indicates that two faraday/mole of **5** is involved in the oxidation step. The other redox waves were assumed to involve one electron per molecule according to the relative peak heights in the voltammogram. The large potential difference between the first and second reduction peaks (over 600 mV) implies that there is good electronic interaction between the two tetra-osmium metal cores, through the azo-ligand in this novel cyclic structure. This kind of electronic interaction also appears in some organometallic dimers.[45−50]

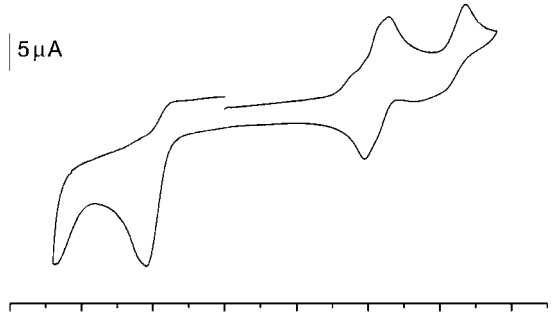

Figure 9. Cyclic voltammogram of $[Os_4(\mu\text{-}H)_4(CO)_{10}\{\mu\text{-}\eta^2\text{-}NC_5H_4(N{=}N)C_5H_4N\}]_2$ (**5**) in CH_2Cl_2 containing 0.1 mol·dm^{-3} Bu_4NPF_6; glassy carbon working electrode, platinum auxiliary electrode and $Ag/AgNO_3$ reference electrode (Ag^+ 0.1 mol·dm^{-3}; scan rate, 100 mV·s^{-1})

There is a completely charged delocalization over two redox centers, while the azo-ligand acts as a conductor. As one metal core receives one electron, the cyclic structure become more electron rich, making the second reduction of another metal core more difficult. The cyclic structure exhibits remarkably flexible redox behavior comparable to **2**, able to accommodate the addition of one electron without gross structural changes. Furthermore, it shows that both reduction and oxidation are more likely to occur in compound **5** than in compound **1**, as the extra charge is shared by two metal cores through the bridging azo-ligands. This is consistent with the 190 mV positive and 90 mV negative shift in cathodic and anodic wave values in comparison to the corresponding value observed in **1**.

Experimental Section

General: All reactions and manipulations were carried out under argon using standard Schlenk techniques, except for the chromatographic separations. Solvents were purified by standard procedures and distilled prior to use.[51] Reactions were monitored by both IR spectroscopy and analytical thin-layer chromatography (Merck Kieselgel 60 F_{254}) and the products were separated by thin-layer chromatography on plates coated with silica (Merck Kieselgel 60 F_{254}).

Materials: All chemicals, unless otherwise stated, were purchased commercially and used as received. $[Os_4(\mu\text{-}H)_4(CO)_{12}]$,[52−54] $[Os_4(\mu\text{-}H)_4(CO)_{10}(NCMe)_2]$,[26] ligand 2,2′-azopyridine,[55] and 3,3′-azopyridine[55] were prepared by literature methods.

Instrumentation: Infrared spectra were recorded on a Bio-Rad FTS-135 IR spectrometer, using 0.5 mm calcium fluoride solution cells. − ^{1}H NMR and ^{1}H-^{1}H COSY spectra were obtained on a Bruker DPX300 spectrometer using CD_2Cl_2 and referenced to $SiMe_4$ (δ = 0), variable-temperature ^{1}H NMR spectra on a Bruker DPX500 spectrometer. − Positive ionization fast atom bombardment (FAB) mass spectra were recorded on a Finnigan MAT 95 mass spectrometer, using *m*-nitrobenzyl alcohol as matrix solvent. − Electronic absorption spectra were obtained with a Hewlett−Packard 8453 diode array UV/Vis spectrophotometer, using quartz cells, with 1 cm path length at room temperature. − Microanalyses were performed by Butterworth Laboratories, UK.

Reaction of $[Os_4(\mu\text{-}H)_4(CO)_{12}]$ with 4-(2-Pyridylazo)-*N*,*N*-dimethylaniline: The complex $[Os_4(\mu\text{-}H)_4(CO)_{12}]$ (110 mg, 0.1 mmol) was dissolved in dichloromethane (50 cm^3) and stirred with one equivalent of 4-(2-pyridylazo)-*N*,*N*-dimethylaniline (22.6 mg, 0.1 mmol) at 0 °C. Two equivalent of trimethylamine *N*-oxide (Me_3NO) were added dropwise over 20 min. After the reaction had proceeded at ambient temperature for 18 h, the initial yellow solution changed to dark brown. The solvent was removed under reduced pressure and the residue subjected to TLC with *n*-hexane/dichloromethane (1:1, v/v) as eluent. Two new products were isolated, in the following order of elution: dark red $[Os_4(\mu\text{-}H)_4(CO)_{11}\{NC_5H_4(N{=}N)C_6H_4NMe_2\}]$ (**1**, R_f = 0.85, 44 mg, 0.034 mmol, 34%). IR [ν(CO)/cm^{-1}, *n*-hexane]: $\tilde{\nu}$ = 2091 w, 2060 s, 2051 m, 2032 m, 2005 m, 1985 m. − ^{1}H NMR (CD_2Cl_2): at 298 K δ = −24.06 (s, 1 H, Os−H), −18.65 (s, 1 H, Os−H), −18.06 (s, 2 H, Os−H), 1.67 (s, 3 H, methyl), 2.04 (s, 3 H, methyl), 6.84 (m, 4 H, pyridyl), 8.01 (m, 4 H, phenyl); at 233 K, **1a:** δ = −24.01 (s, 1 H, Os−H), −18.63 (s, 1 H, Os−H), −18.10 (s, 2 H, Os−H); **1b:** δ = −25.53 (s, 1 H, Os−H), −18.86 (s, 1 H, Os−H), −17.95 (s, 1 H, Os−H), −16.93 (s, 1 H, Os−H). − MS (positive FAB): *m*/*z* (%) = 1073 [M$^+$ − PNNDA]. − $C_{24}H_{18}N_4O_{11}Os_4$ (1299.3): calcd. C 22.20, H 1.39, N 4.31; found C 22.3, H 1.5, N 4.2; and dark blue (**2**, R_f = 0.7, 19 mg, 0.015 mmol, 15%). − IR [ν(CO)/cm^{-1}, *n*-hexane]: $\tilde{\nu}$ = 2087 w, 2077 m, 2050 vs, 2019 s, 2000 s, 1983 m. − ^{1}H NMR (CD_2Cl_2): at 298 K δ = −19.64 (br. s, Os−H), −19.28 (br. s, Os−H), −18.71 (br. s, Os−H), 2.82[s, 6 H, methyl], 6.95 (d, J_{HH} = 9.4 Hz, 2 H, phenyl], 7.60 (d, J_{HH} = 6.4 Hz, 1 H, pyridyl], 8.28 (m, 3 H, pyridyl and phenyl), 8.52 (d, J_{HH} = 8.1 Hz, 1 H, pyridyl], 9.36 (d, J_{HH} = 5.4 Hz, 1 H, pyridyl]; at 223 K, **2a:** δ = −20.06 (s, 1 H, Os−H),

−19.28 (s, 1 H, Os−H), −17.92 (s, 1 H, Os−H), −17.31 (s, 1 H, Os−H); **2b:** δ = −20.71 (s, 1 H, Os−H), −19.65 (s, 1 H, Os−H), −19.34 (s, 1 H, Os−H), −19.13 (s, 1 H, Os−H); **2c:** δ = −20.28 (s, 1 H, Os−H), −20.19 (s, 1 H, Os−H), −19.79 (s, 1 H, Os−H), −19.18(s, 1 H, Os−H); **2d:** δ = −22.66 (s, 1 H, Os−H), −22.13 (s, 1 H, Os−H), −18.37 (s, 1 H, Os−H), −18.04 (s, 1 H, Os−H). − MS (positive FAB): *m*/*z* (%) = 1271 $[M]^+$. − $C_{23}H_{18}N_4O_{10}Os_4$ (1271.3): calcd. C 21.73, H 1.43, N 4.41; found C 21.6, H 1.3, N 4.4.

$[Os_4(\mu\text{-}H)_3(CO)_{10}\{\mu\text{-}\eta^3\text{-}Et_2NC_6H_3(O)(N{=}N)C_5NH_3Br\}]$ (3): The complex $[Os_4(\mu\text{-}H)_4(CO)_{12}]$ (110 mg, 0.1 mmol) was dissolved in dichloromethane (50 cm^3) and mixed with one equivalent of 2-(5-bromo-2-pyridylazo)-5-(diethylamino)phenol (34.9 mg, 0.1 mmol) at 0 °C. Two equivalent of trimethylamine *N*-oxide were added dropwise. The yellow mixture was stirred for 12 h, which resulted in the formation of a deep purple solution. The solvent was pumped off and the residue purified by chromatography on TLC plates with *n*-hexane/diethyl ether (3:2, v/v) as eluent. Recrystallization from dichloromethane/*n*-hexane afforded purplish-red crystals. (R_f = 0.4, 11 mg, 0.008 mmol, 8%). − IR [ν(CO)/cm^{-1}, *n*-hexane]: $\tilde{\nu}$ = 2087 w, 2055 s, 2026 s, 2010 s. − ^{1}H NMR (CD_2Cl_2): δ = −20.58 (s, 1 H, Os−H), −16.43 (s, 1 H, Os−H), −13.17 (s, 1 H, Os−H), 1.32 (m, 6 H, CH_3), 3.50 (m, 4 H, CH_2), 5.99 (d, J_{HH} = 2.5 Hz, 1 H, phenyl), 6.47 (dd, J_{HH} = 9.8 Hz, 1 H, phenyl), 7.04 (d, J_{HH} = 9.4 Hz, 1 H, phenyl), 7.09 (d, J_{HH} = 9.2 Hz, 1 H, pyridyl), 7.80 (dd, J_{HH} = 9.0 Hz, 1 H, pyridyl), 9.05 (d, J_{HH} = 8.2 Hz, 1 H, pyridyl). − MS (positive FAB): *m*/*z* (%) = 1392 $[M]^+$. − $C_{25}H_{19}BrN_4O_{11}Os_4$ (1392.2): calcd. C 21.57, H 1.38, N 4.02; found C 21.7, H 1.5, N 3.9.

$[Os_4(\mu\text{-}H)_2(CO)_{10}\{\mu\text{-}\eta^3\text{-}NC_5H_4(N{=}N)C_5H_4N\}]$ (4): The complex $[Os_4(\mu\text{-}H)_4(CO)_{10}(NCMe)_2]$ (110 mg, 0.1 mmol) was dissolved in dichloromethane (50 cm^3) and stirred with one equivalent of 2,2′-azopyridine (18.4 mg, 0.1 mmol) at ambient temperature. After 5 h, the solvent was removed under reduce pressure. The residue was purified by chromatography on TLC plates with *n*-hexane/dichloromethane (1:1, v/v) as eluent. Recrystallization from chloroform/*n*-hexane afforded blue crystals. (R_f = 0.3, 15 mg, 0.012 mmol, 12%). − IR [ν(CO)/cm^{-1}, *n*-hexane]: $\tilde{\nu}$ = 2083 m, 2068 w, 2047 s, 2035 s, 2021 w, 2001 vs, 1977 w. − ^{1}H NMR (CD_2Cl_2): δ = −21.02 (s, 1 H, Os−H), −13.02 (s, 1 H, Os−H), 6.49 (td, J_{HH} = 6.6 Hz, 1 H, pyridyl), 7.25 (td, J_{HH} = 6.8 Hz, 2 H, pyridyl), 7.97 (m, 2 H, pyridyl), 8.17 (d, J_{HH} = 8.3 Hz, 1 H, pyridyl), 8.76 (d, J_{HH} = 5.7 Hz, 1 H, pyridyl), 8.83 (d, J_{HH} = 6.8 Hz, 1 H, pyridyl). − MS (positive FAB): *m*/*z* (%) = 1227 $[M]^+$. − $C_{20}H_{10}N_4O_{10}Os_4$ (1227.2): calcd. C 19.57, H 0.82, N 4.57; found C 19.7, H 0.9, N 4.5.

$[Os_4(\mu\text{-}H)_4(CO)_{10}\{\mu\text{-}\eta^2\text{-}NC_5H_4(N{=}N)C_5H_4N\}]_2$ (5): The complex $[Os_4(\mu\text{-}H)_4(CO)_{10}(NCMe)_2]$ (110 mg, 0.1 mmol) was dissolved in dichloromethane (50 cm^3) and stirred with one equivalent of 3,3′-azopyridine (18.4 mg, 0.1 mmol) at ambient temperature. After 24 h, the initial yellow solution changed to dark brown. The solvent was then remove in vacuo and the residue was purified by chromatography on TLC plates with *n*-hexane/dichloromethane (1:1, v/v) as eluent. Recrystallization from tetrahydrofuran/*n*-hexane afforded brown crystals. (R_f = 0.45, 29.5 mg, 0.012 mmol, 12%). − IR [ν(CO)/cm^{-1}, dichloromethane]: $\tilde{\nu}$ = 2074m, 2047s, 2028vs, 2001s, 1976w. − ^{1}H NMR (CD_2Cl_2): δ = −20.09 (s, 2 H, Os−H), −17.05 (s, 2 H, Os−H), −16.46 (s, 2 H, Os−H), −15.53 (s, 2 H, Os−H), 7.50 (dd, J_{HH} = 8.2 Hz, 2 H, pyridyl), 7.71 (dd, J_{HH} = 8.0 Hz, 2 H, pyridyl), 8.34 (dt, J_{HH} = 6.9 Hz, 2 H, pyridyl), 8.62 (dt, J_{HH} = 8.6 Hz, 2 H, pyridyl), 9.10 (d, J_{HH} = 2.1 Hz, 2 H, pyridyl), 9.24 (td, J_{HH} = 5.2 Hz, 4 H, pyridyl), 9.52 (d, J_{HH} = 1.9 Hz, 2 H, pyridyl). − MS (positive FAB): *m*/*z* (%) = 2458 $[M]^+$. − $C_{40}H_{24}N_8O_{20}Os_8$ (2458.3): calcd. C 19.54, H 0.98, N 4.56; found C 19.4, H 1.0, N 4.6.

Electrochemical Studies: Electrochemical measurements were performed with EG&G Princeton Applied Research (PAR) Model 273A potentiostat, connected to an interfaced computer employing PAR 270 electrochemical software. Cyclic voltammograms were obtained using a gas (argon) sealed two-compartment cell equipped

Table 4. Crystal data and data collection parameters for compounds **1**−**5**

	1	**2**	**3**	**4**	**5**
Empirical formula	$C_{24}H_{18}N_4O_{11}Os_4$	$[C_{23}H_{18}N_4O_{10}Os_4]\cdot 1CHCl_3$	$[C_{25}H_{19}N_4O_{11}Br_1Os_4]\cdot 1CH_2Cl_2$	$C_{20}H_{10}N_4O_{10}Os_4$	$[C_{40}H_{24}N_8O_{20}Os_8]\cdot 4C_4H_8O$
Molecular mass	1299.23	1390.59	1477.08	1227.12	2746.70
Crystal color, habit	red, block	blue, block	purple, block	blue, block	brown, block
Crystal dimensions [mm]	0.22 × 0.22 × 0.10	0.22 × 0.17 × 0.14	0.22 × 0.19 × 0.12	0.23 × 0.12 × 0.22	0.23 × 0.22 × 0.25
Crystal system	monoclinic	triclinic	triclinic	monoclinic	monoclinic
Space group	$P2_1/n$ (no. 14)	$P\bar{1}$ (no. 2)	$P\bar{1}$ (no. 2)	$P2_1/n$ (no. 14)	$P2_1/n$ (no. 14)
a [Å]	8.2310(8)	9.8510(9)	9.792(1)	12.243(1)	13.104(1)
b [Å]	27.885(1)	12.644(1)	11.709(1)	12.472(1)	16.423(1)
c [Å]	13.8710(8)	15.557(1)	17.632(1)	16.621(1)	17.853(1)
α [Å]		67.020(5)	77.40(1)		
β [Å]	105.710(5)	81.690(5)	77.02(1)	93.40(1)	107.40(2)
γ [Å]		69.110(5)	68.33(1)		
U [$Å^3$]	3064.8(3)	1666.6(3)	1810.2(3)	2533.5(3)	3666.3(6)
Z	4	2	2	4	2
D_c [g cm^{-3}]	2.816	2.771	2.710	3.217	2.488
μ(Mo-K_α) [cm^{-1}]	165.82	154.86	152.97	200.46	138.70
Reflections collected	19241	19107	11225	15648	22910
Unique reflections	7074	7480	7789	5956	8538
Observed reflections [I>1.5σ(I)]	4098	6262	5890	4783	3713
R	0.053	0.034	0.039	0.055	0.066
R_w	0.061	0.043	0.041	0.065	0.054
Goodness of fit, *S*	1.09	1.33	1.13	1.82	1.09

with a glassy carbon working electrode (Bioanalytical), a platinum wire auxiliary electrode (Aldrich), and an $Ag/AgNO_3$ reference electrode (Bioanalytical) at room temperature; 0.1 mol·dm^{-3} *n*-tetrabutylammonium hexafluorophosphate (TBAHFP) in anhydrous deoxygenated CH_2Cl_2 was used as a supporting electrolyte. Ferrocene was added at the end of each experiment as an internal standard. Potential data (vs. $Ag/AgNO_3$) were checked against the ferrocene (0/+1) couple; under the actual experimental conditions the ferrocene/ferrocenium couple is located at +0.13 V. Bulk electrolyses were carried out in a gas-tight cell consisting of three chambers separated at the bottom by fine frits, with a carbon cloth (80 mm^2) working electrode in the middle, and $Ag/AgNO_3$ reference and Pt gauze auxiliary electrodes in the lateral chambers. The working potentials (E_w) for reduction and oxidation processes were ca. 0.15 V more negative and more positive than the corresponding electrode potential (E_p), respectively; all coulometric experiments were performed in duplicate.

Crystallography: Crystals suitable for X-ray analyses were glued on glass fibers with epoxy resin or sealed in a 0.3 mm glass capillary. Intensity data were collected at ambient temperature using a Bruker SMART CCD 1000 diffractometer with graphite monochromated Mo-K_α radiation using ω scan type. Details of the intensity data collection and crystal data are given in Table 4. The data were corrected for Lorentz and polarization effects. The structure were solved by direct methods[56] and expanded using Fourier techniques.[57] Some non-hydrogen atoms were refined anisotropically, while the rest were refined isotropically. Hydrogen atoms were included but not refined. All calculations were performed by using the teXsan[58] crystallographic software package of Molecular Structure Corporation.

Crystallographic data (excluding structure factors) for the structures reported in this paper have been deposited with the Cambridge Crystallographic Data Centre as supplementary publication nos. CCDC-163743 to CCDC-163747. Copies of the data can be obtained free of charge on application to CCDC, 12 Union Road, Cambridge CB2 1EZ, UK. [Fax: (internat.) +44 (0)1223/336033; E-mail: deposit@ccdc.cam.ac.uk].

Acknowledgments

We gratefully acknowledge financial support from the Hong Kong Research Grants Council and the University of Hong Kong. Y. Li acknowledges the receipt of a postgraduate studentship, administered by the University of Hong Kong.

[1] A. K. Ghosh, P. Majumdar, L. R. Falvello, G. Mostafa, S. Goswani, *Organometallics* **1999**, *18*, 5086−5090.
[2] M. A. Aubart, R. G. Bergman, *Organometallics* **1999**, *18*, 811−813.
[3] S. D. Gray, J. L. Thorman, V. A. Adamian, K. M. Kadish, L. K. Woo, *Inorg. Chem.* **1998**, *37*, 1−4.
[4] F. Y. Petillon, P. Scholhammer, J. Talarmin, *Inorg. Chem.* **1999**, *38*, 1954−1955.
[5] M. A. Lockwood, P. E. Fanwick, O. Eisenstein, I. P. Rothwell, *J. Am. Chem. Soc.* **1996**, *118*, 2762−2763.
[6] B. Hansert, M. Tasi, A. Tiripicchio, M. T. Camellini, H. Vahrenkamp, *Organometallics* **1991**, *10*, 4070−4073.
[7] M. Tasi, A. K. Powell, H. Vahrenkamp, *Chem. Ber.* **1991**, *124*, 1549−1557.
[8] H. Bantel, B. Hansert, A. K. Powell, M. Tasi, H. Vahrenkamp, *Angew. Chem. Int. Ed. Eng.* **1989**, *28*, 1059−1060.
[9] J. A. Smieja, J. E. Gozum, W. L. Gladfelter, *Organometallics* **1987**, *6*, 1311−1317.
[10] B. Hansert, H. Vahrenkamp, *Chem. Ber.* **1993**, *126*, 2017−2022.
[11] B. Hansert, H. Vahrenkamp, *Chem. Ber.* **1993**, *126*, 2023−2026.
[12] B. Hansert, A. K. Powell, H. Vahrenkamp, *Chem. Ber.* **1991**, *124*, 2697−2704.
[13] E. J. Wucherer, M. Tasi, B. Hansert, A. K. Powell, M. T. Garland, J. F. Halet, J. Y. Saillard, H. Vahrenkamp, *Inorg. Chem.* **1989**, *28*, 3564−3572.
[14] Y. K. Au, K. K. Cheung, W. T. Wong, *Inorg. Chim. Acta* **1995**, *238*, 193−195.
[15] F. S. Kong, W. T. Wong, *J. Organomet. Chem.* **1999**, *589*, 180−190.
[16] J. A. Smieja, J. E. Gozum, W. L. Gladfelter, *Organometallics* **1986**, *5*, 2154−2155.
[17] B. Hansert, H. Vahrenkamp, *Chem. Ber.* **1993**, *126*, 2011−2016.
[18] K. Majumder, S. M. Peng, Samaresh Bhattacharya, *J. Chem. Soc., Dalton Trans.* 2001, 284−288.
[19] W. T. Wong, T. S. Wong, *J. Organomet. Chem.* **1997**, *542*, 29−33.
[20] J. C. Cyr, J. A. DeGray, D. K. Gosser, E. S. Lee, P. H. Rieger, *Organometallics* **1985**, *4*, 950−951.
[21] J. E. Cyr, P. H. Rieger, *Organometallics* **1991**, *10*, 2153−2159.
[22] T. M. Bockman, J. K. Kochi, *J. Am. Chem. Soc.* **1987**, *109*, 7725−7735.
[23] D. Osella, L. Pospisil, J. Fiedler, *Organometallics* **1993**, *12*, 3140−3144.
[24] Y. Y. Choi, W. T. Wong, *J. Organomet. Chem.* **1999**, *573*, 189−201.
[25] K. S. Y. Leung, Y. Li, *Inorg. Chem. Commun.* **1999**, *2*, 599−603.
[26] Y. Y. Choi, PhD Thesis, The University of Hong Kong, **1998**.
[27] M. R. Churchill, R. A. Lashewycz, *Inorg. Chem.* **1979**, *18*, 1926−1930.
[28] B. F. G. Johnson, J. Lewis, W. J. H. Nelson, M. A. Pearsall, P. R. Raithby, M. J. Rosales, *J. Chem. Soc., Dalton Trans.* **1987**, 327−333.
[29] T. S. Wong, unpublished results.
[30] N. E. Leadbeater, J. Lewis, P. R. Raithby, G. N. Ward, *J. Chem. Soc., Dalton Trans.* **1997**, 2511−2516.
[31] A. J. Deeming, C. Whittaker, A. J. Arce, Y. D. Sanctis, *J. Organomet. Chem.* **1997**, *540*, 67−76.
[32] W. Y. Wong, S. Chan, W. T. Wong, *J. Organomet. Chem.* **1995**, *493*, 229−237.
[33] W. Y. Wong, W. T. Wong, *J. Chem. Soc., Dalton Trans.* **1996**, 1853−1856.
[34] C. E. Housecroft, personal communication.
[35] B. F. G. Johnson, F. J. Lahoz, J. Lewis, N. D. Prior, P. R. Raithby, W. T. Wong, *J. Chem. Soc., Dalton Trans.* **1992**, 1701−1708.
[36] M. M. Zulu, A. J. Lees, *Inorg. Chem.* **1988**, *27*, 3325−3331.
[37] J. Granifo, M. E. Vargas, E. S. Dodsworth, D. H. Farrar, S. S. Fielder, A. B. P. Lever, *J. Chem. Soc., Dalton Trans.* **1996**, 4369−4378.
[38] E. S. Dodsworth, A. B. P. Lever, *Inorg. Chem.* **1990**, *29*, 499−503.
[39] P. Suppan, N. Ghoneim (Eds.), *Solvatochromism*, The Royal Society of Chemistry, (London) **1997**.
[40] C. Reichardt, *Chem. Rev.* **1994**, *94*, 2319−2358.
[41] F. Effenberger, F. Wurthner, *Angew. Chem. Int. Ed. Engl.* **1993**, *32*, 719−721.
[42] E. Buncel, S. Rajagopal, *Acc. Chem. Res.* **1990**, *23*, 226−231.
[43] J. Heinze, *Angew. Chem. Int. Ed. Eng.* **1984**, *11*, 831−847.
[44] S. R. Drake, *Polyhedron* **1990**, *9*, 455−474.
[45] D. Osella, L. Milone, C. Nervi, M. Ravera, *J. Organomet. Chem.* **1995**, *488*, 1−7.
[46] D. Osella, O. Gambino, C. Nevi, M. Ravera, D. Bertolino, *Inorg. Chim. Acta* **1993**, *206*, 155−161.
[47] D. Osella, J. Hanzlik, *Inorg. Chim. Acta.* **1993**, *213*, 311−317.

[48] J. Hock, A. M. W. C. Thompson, J. A. McCleverty, M. D. Ward, *J. Chem. Soc., Dalton Trans.* **1996**, 4257−4263.
[49] R. D. Adams, B. Qu, *J. Organomet. Chem.* **2001**, *620*, 303−307.
[50] R. D. Adams, B. Qu, *J. Organomet. Chem.* **2001**, *619*, 271−274.
[51] D. D. Perrin, W. L. F. Armarego, Purification of Laboratory Chemicals, 3rd ed., Pergamon, Oxford, **1988**.
[52] H. D. Kaesz, S. A. R. Knox, J. W. Koepke, R. B. Saillant, *J. Chem. Soc., Chem. Commun.* **1971**, 477.
[53] B. F. G. Johnson, J. Lewis, P. R. Raithby, G. M. Scheldrick, K. Wong, *J. Chem. Soc., Dalton Trans.* **1978**, 673−676.
[54] C. Zuccaro, G. Pampaloni, F. Calderazzo, *Inorg. Synth.* **1989**, *26*, 293−295.
[55] E. V. Brown, G. R. Granneman, *J. Am. Chem. Soc.* **1975**, *97*, 621−627.
[56] *SHELXS86*: G. M. Sheldrick, in: *Crystallographic Computing 3* (Eds. G. M. Sheldrick, C. Kruger, R. Goddard), Oxford University Press, **1985**, pp. 175−189.
[57] *DIRDIF94*: P. T. Beurskens, G. Admiraal, G. Beurskens, W. P. Bosman, R. de Gelder, R. Israel, J. M. M. Smits, **1994**; *The DIRDIF-94 program system*, Technical Report of the Crystallography Laboratory, University of Nijmegen, The Netherlands.
[58] *TeXsan*: Crystal Structure Analysis Package, Molecular Structure Corporation (**1985** and **1992**).

Received May 21, 2001
[I01184]